EPJ manuscript No.
(will be inserted by the editor)

Nuclear radius systematics of Kr isotopes studied via their interaction cross-sections at relativistic energies

T. Yamaguchi[1], T. Suzuki[1], T. Ohnishi[2], K. Sümmerer[3], F. Becker[3], M. Fukuda[4], H. Geissel[3], M. Hosoi[1], R. Janik[5], K. Kimura[6], S. Mandal[3], G. Münzenberg[3], S. Nakajima[1], T. Ohtsubo[7], A. Ozawa[8], A. Prochazka[5], M. Shindo[9], B. Sitar[5], P. Strmen[5], T. Suda[2], K. Sugawara[1], I. Szarka[5], A. Takisawa[7], M. Takechi[4] and K. Tanaka[2]

[1] Department of Physics, Saitama University, Saitama 338-8570, Japan
[2] The Institute of Physical and Chemical Research (RIKEN), Saitama 351-0198, Japan
[3] Gesellschaft für Schwerionenforschung (GSI), Planckstrasse 1, D-64291 Darmstadt, Germany
[4] Department of Physics, Osaka University, Osaka 560-0043, Japan
[5] Faculty of Mathematics and Physics, Comenius University, 84215 Bratislava, Slovak Republic
[6] Nagasaki Institute of Applied Science, Nagasaki 851-0193, Japan
[7] Department of Physics, Niigata University, Niigata 950-2181, Japan
[8] Department of Physics, University of Tsukuba, Ibaraki 305-8577, Japan
[9] Department of Physics, University of Tokyo, Tokyo 113-0033, Japan

Received: 31 August 2006 / Revised version: date

Abstract. The interaction cross-sections of neutron-deficient ^{72,76,80}Kr isotopes have been measured by use of the transmission method at relativistic energies. Based on the Glauber model analysis effective root-mean-square matter radii of these nuclei have been determined for the first time. A systematic evolution of the matter radii in the mass $A \sim 70$ region is discussed and compared with that of light nuclei.

PACS. 21.10.Gv Mass and neutron distributions – 25.60.Dz Interaction and reaction cross sections – 27.50+e 59(less-than-or-equal-to)A(less-than-or-equal-to)89

1 Introduction

Precision measurements of the interaction cross-sections ($\sigma_{\rm I}$) at relativistic energies $\sim$1 AGeV allow us to derive nuclear matter radii [1]. Since nuclear matter radii are directly related to the density distributions, the measurements of the interaction cross-sections are a good tool to search for unusual nuclear structures such as halo and skin. We have performed several experiments and have successfully determined nuclear matter radii of unstable nuclei in the light region [2–7]. Such systematic studies have led up to the discovery of new magic number $N = 16$ in the light neutron-rich nuclei [8] and the evidence for the proton skins in proton-rich Ar isotopes [7]. So far nuclear matter radii studied via the interaction cross-sections have been determined up to the mass $A \sim 40$ region.

Recently anomalous behavior of the matter radii of proton-rich Ga, Ge, As, Se, and Br nuclei was reported by measuring the reaction cross-sections at the intermediate beam energies [9,10]. The authors of Ref. [9,10] claim that a decrease of the root-mean-square (rms) radii with increasing neutron number for all isotopic series and their correlation with deformation was observed. Proton-rich Kr isotopes close to the $N = Z$ line, including the self-conjugate nucleus ^{72}Kr, attract a particular interest in their structures. These isotopes are located in the middle of the fp shell, around the shell gaps in the deformed shell model potential, where competing prolate-spherical or oblate-spherical shape transitions have been predicted for many years. By adding or removing a few nucleons to a nucleus nuclear shape can change dramatically. Recent Coulomb excitation experiments [11–14] have indicated large deformations in this region, and even the evidence of the shape coexistence for ^{72,74}Kr. Nuclear shape is determined by the interplay between macroscopic and microscopic effects. Nuclear matter radii would provide macroscopic information to account for the ground-state properties of these nuclei. In this report, therefore, we present preliminary results of the effective rms matter radii of neutron-deficient ^{72,76,80}Kr isotopes studied via the interaction cross-sections measured at the relativistic energies, and discuss the systematics of the matter radii in this region.

2 Experimental

The experiment was performed at the fragment separator FRS at GSI, Darmstadt [15]. A primary beam of ^{80}Kr accelerated by the SIS synchrotron to an energy of 1.05 AGeV impinged on a Be target at the entrance (F0) of FRS to produce secondary beams of ^{72,76}Kr through the

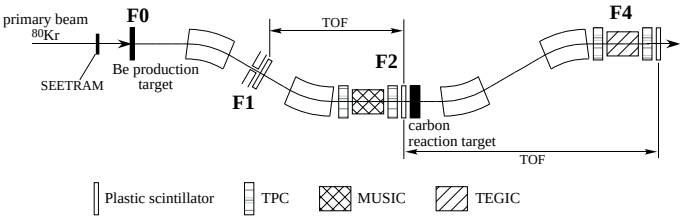

Fig. 1. Experimental setup at the fragment separator FRS.

projectile fragmentation reaction. A total of three different settings of FRS were used to select ^{72,76,80}Kr as the central beams. A 2 g/cm^2 thick Be target was used for the ^{72}Kr setting, 1 g/cm^2 thick for ^{76}Kr, and no production target for ^{80}Kr. A typical intensity of 5×10^8 particles per spill was used to produce ^{72}Kr. Each spill lasted for approximately 800 ms and was extracted from SIS every 2 s.

The experimental setup is sketched in Fig. 1. The secondary electron transmission monitor SEETRAM [16] in front of the target was used to determine the primary beam intensity. At the first focus (F1), we placed a scintillation counter (thickness $t = 3$ mm) to obtain the start signal for a time-of-flight (TOF) measurement. This detector consisted of a plastic scintillator (BC418) and photomultipliers (R2083 Hamamatsu PMT). Two PMT were attached on both ends of the scintillator via straight shaped light guides [17]. Additional high voltages were applied to the last three dynodes of both PMT to keep the amplification gain constant under the condition of high rate irradiation at F1. It also served as an active slit for momentum definition ($\Delta p/p = \pm0.2\%$). At the momentum–dispersive intermediate focus (F2) of FRS (dispersion: 7 cm/%), we installed another plastic scintillation counter (BC420, width $w = 120$ mm and $t = 3$ mm) to obtain the TOF stop signal (flight path length $l = 17.8$ m). The TOF resolution of 33 ps (FWHM) obtained for the primary beam, as shown in Fig. 2(a), was sufficient to separate the mass number A of the particles of interest unambiguously. Here it should be noted that the lifetimes of isomeric states, such as $\tau = 4.53(59)$ ps for 2_1^+ state of ^{72}Kr [14], are safely shorter than the time-of-flight between F0 and F2.

The fragment nuclear charge number Z was determined by an energy-loss (ΔE) measurement with the ionization chamber, MUSIC [18]. It was calibrated with the primary beam for the nuclear charge $Z = 36$ (see Fig. 2(b)). The ΔE resolution of 0.6 % in σ was obtained, corresponding to the Z-resolving power of $\Delta Z = 0.33$ (FWHM). Additionally, we positioned two time projection chambers (TPC) developed at Comenius University in Slovakia [19] at F2 to tune the separator and to monitor the beam emittance. The position information at the foci F1 and F2 together with the magnetic field in the second dipole magnet gave $B\rho$ of the fragments. This allowed us to calculate A/Z and Z from $B\rho$, TOF, and ΔE, providing complete particle identification. The fragments, ^{72,76}Kr, were thus produced, separated in the first half of the FRS with a selection of their mass-over-charge ratios, and delivered to the reaction target located at F2.

A 2.30 g/cm^2 thick carbon was used for the reaction target. Thickness non-uniformity of the carbon target was negligible. The setup at F4 is essentially the same as that at F2. We placed two TPC, an ionization chamber, and a plastic scintillation counter (BC420, $w = 200$ mm and $t = 3$ mm). The scintillation counter at F2 served as a TOF start counter and the scintillator at F4 as a stop. We employed the titled-electrode gas ionization chamber (TEGIC)[20], developed at RIKEN, for the energy-loss measurement at F4. The ionization chamber, TEGIC, consists of a stacked configuration of grid-less parallel plate gas ionization chambers with thin anode-cathode gaps. The high-rate capability of this chamber was realized by adopting bipolar shaping of multi-sampled anode signals and by the suitable choice of a counter gas Ar-CH_4 (90%, 10%). The ΔE resolution of 1.0 % in σ was obtained for the ^{80}Kr beam. Two TPC were used to tune the separator. In a similar manner with F2, $B\rho$, TOF, and ΔE provided complete particle identification in the second half of the FRS.

The principle of the measurements was based on the transmission method. The first and the second half of the FRS are used as a spectrometer to identify incom-

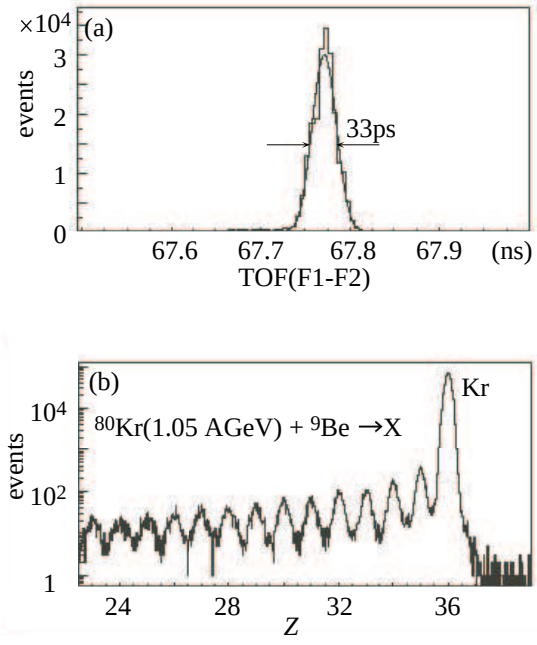

Fig. 2. (a) Time of flight spectrum of primary beam ^{80}Kr between the scintillators at F1 and F2. (b) Energy-loss spectrum for ^{80}Kr fragmentation measured with the ionization chamber MUSIC at F2. The separator was tune to calibrate the MUSIC by using the $Z = 36$ beam.

ing and outgoing particles, respectively. The interaction cross-section is derived from the equation,

$$\sigma_I = -\frac{1}{t} ln \left(\frac{\Gamma}{\Gamma_0} \right) \quad (1)$$

where Γ is the ratio of the numbers of non-interacting outgoing particles relative to the incoming particles. Γ_0 is the same for an empty target measurement which cancels out spurious effects caused by unwanted events reacted in the detectors. t is the thickness of the carbon target. For the transmission method it is crucial to count accurately all non-interacting particles downstream of the reaction target. In order to ensure full transmission in the second half of the FRS a small emittance cut was applied for the incident beams based on the position information of two TPC at F2.

3 Data analysis

Based on the Glauber model in the optical-limit approximation [21] effective root-mean-square (rms) matter radii are deduced from the interaction cross-sections. The Glauber model describes the reaction cross-section (σ_R) as

$$\sigma_R = \int (1 - T(b)) d^2b \quad (2)$$

$$T(b) = exp \left(-\sigma_{NN} \int \rho_T^z(|\overrightarrow{b} - \overrightarrow{s}|) \rho_P^z(s) d^2s \right) \quad (3)$$

where $T(b)$ is the transmission function, b is the impact parameter. σ_{NN} represents the total nucleon-nucleon cross-sections, and ρ_i^z is the z-integrated density distribution for the target ($i = T$) or the projectile ($i = P$). It should be noted that the interaction cross-sections are almost equal to the reaction cross-sections ($\sigma_R = \sigma_I + \sigma_{inelastic}$) at high energy limit, $\sigma_I \simeq \sigma_R$ [7].

For the target (^{12}C) the Harmonic-Oscillator type density distribution was applied which reproduces the densities of light nuclei well. For the projectiles (^{72,76,80}Kr), Fermi type function was employed as the density distribution,

$$\rho(r) = \frac{\rho_0}{1 + exp\left(\frac{r-R}{a}\right)} \quad (4)$$

where R and a are the half radius and the diffuseness parameter respectively. We fixed the diffuseness parameter to be $a = 0.496$ fm which was obtained from the electron scattering experiment of ^{88}Sr [22]. Preliminary results of the effective rms matter radii of ^{72,76,80}Kr are shown in Fig. 3 together with the rms radii of Ga, Ge, As, Se, and Br measured at GANIL [9,10].

4 Results and discussions

Recently Lima *et al.* [9,10] have measured the reaction cross-sections of proton-rich Ga, Ge, As, Se, and Br isotopes at the intermediate energies. They employed the target-telescope system of the stacked silicon detectors surrounded by the Ge detectors. It was observed that for all isotopes the rms matter radii tend to decrease as the mass number increases, even though the experimental uncertainties were relatively large due to the efficiency corrections for the Ge detectors. The present result of Kr isotopes also supports this behavior of the matter radii. To make clear a systematic evolution of the radii, isotone dependence of the rms radii for $N = 36$ is plotted in Fig. 4. Dotted line shows the $A^{1/3}$ dependence of the radii normalized for Ga. It is clear that the rms radii increase monotonically toward the proton-drip line. This is similar with that of the neutron-rich side where the rms matter radii are getting larger with the increase of the neutron number. Typical example is Li isotopes (see [21] as a review).

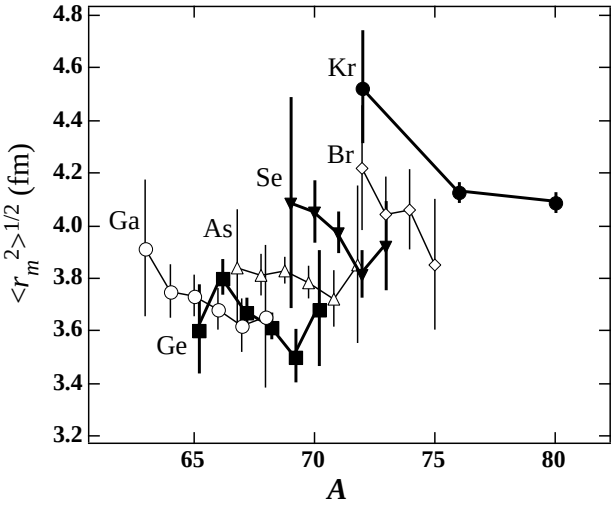

Fig. 3. Effective root-mean-square matter radii of Ga (open circles), Ge (filled squares), As (open triangles), Se (filled inverted triangles), Br (open diamonds) [9], and present results of Kr (filled circles). Each isotope is connected with a straight line for eye guide.

The situation, however, seems different from our observations at the proton-rich side in light nuclei. Suzuki *et al.* measured the interaction cross-sections of Na isotopes and determined their rms matter radii [2]. The authors of Ref. [2] evaluated the neutron skin thickness and discussed the correlation with the separation energy difference. Even at the proton-rich side the radii of Na isotopes tend to decrease monotonically as the mass number decreases. Similar situation for Ar isotopes is observed [7]. This is not the case of course for the proton halo nuclei such as ^{8}B. To establish the evolution of the rms matter radii for the proton-rich side as well as the neutron-rich side, precision measurements of the total reaction cross-sections of unstable nuclei are greatly encouraged. Particular interest is in the radii of heavier nuclei at the proton-rich side.

In summary, we have measured the interaction cross-sections of neutron-deficient ^{72,76,80}Kr isotopes and determined their effective rms matter radii based on the Glauber model analysis in the optical-limit approximation. It was shown that the effective rms matter radii

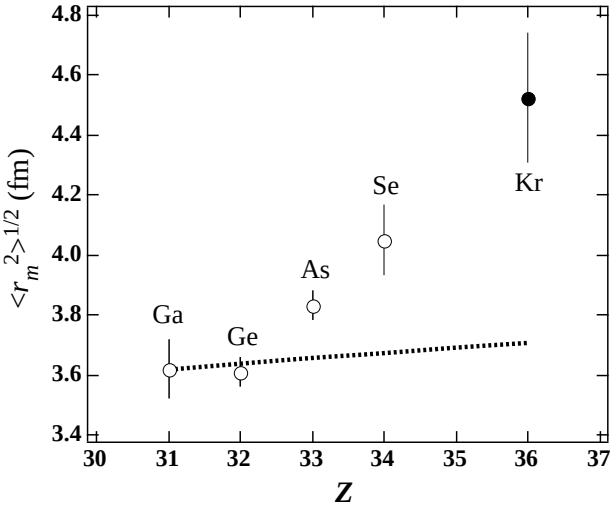

Fig. 4. Isotone dependence of the rms matter radii for $N = 36$. Data of Ga, Ge, As, and Se shown by open circles were taken from Ref. [9]. Dotted line shows the $A^{1/3}$ dependence of the matter radii normalized for Ga.

around the mass $A \sim 70$ at the proton-rich side increase toward the proton-drip line.

Acknowledgments

We thank K.-H. Behr, A. Brünle, K. Burkard, C. Karagiannis, and the members of the FRS group for their technical assistance, and the SIS staff members for stable operations of the accelerators. This work was supported in part by the Japanese Ministry of Education, Science, Sports and Culture by Grant-In-Aid for Scientific Research under Program No. B(2) 16340063, and in part by VEGA, Slovakia.

References

1. I. Tanihata *et al.*, Phys. Lett. B **287**, 307 (1992).
2. T. Suzuki *et al.*, Phys. Rev. Lett. **75**, 3241 (1995).
3. L.V. Chulkov *et al.*, Nucl. Phys. A **603**, 219 (1996).
4. T. Suzuki *et al.*, Nucl. Phys. A **658**, 313 (1999).
5. L.V. Chulkov *et al.*, Nucl. Phys. A **674**, 330 (2000).
6. A. Ozawa *et al.*, Nucl. Phys. A **691**, 599 (2001).
7. A. Ozawa *et al.*, Nucl. Phys. A **709**, 60 (2002).
8. A. Ozawa *et al.*, Phys. Rev. Lett. **84**, 5493 (2000).
9. G.F. Lima *et al.*, Nucl. Phys. A **735**, 303 (2004).
10. A. Lépine-Szily *et al.*, Eur. Phys. J. A **25**, 227 (2005).
11. C. Chandler *et al.*, Phys. Rev. C **56**, 2924 (1997).
12. E. Bouchez *et al.*, Phys. Rev. Lett. **90**, 082502 (2003).
13. J.J. Valiente-Dobón *et al.*, Phys. Rev. Lett. **95**, 232501 (2005).
14. A. Gade *et al.*, Phys. Rev. Lett. **95**, 022502 (2005).
15. H. Geissel *et al.*, Nucl. Instr. Methods B**70**, 286 (1992).
16. C. Ziegler *et al.*, GSI Scientific Report 1990, pp. 291 (1991).
17. S. Nishimura *et al.*, Nucl. Instr. Methods A **510**, 377 (2003).
18. A. Stolz *et al.*, Phys. Rev. C **65**, 064603 (2000).
19. V. Hlinka *et al.*, Nucl. Instr. Methods A **419**, 503 (1998).
20. K. Kimura *et al.*, Nucl. Instr. Methods A **538**, 608 (2005).
21. A. Ozawa *et al.*, Nucl. Phys. A **693**, 32 (2001).
22. H. de Vries *et al.*, Atomic Data and Nuclear Data Tables **36**, 495 (1987).